Electronic Supplementary Material (ESI) for Inorganic Chemistry Frontiers.

Supporting Information
A Mass-Producible Polyoxovanadate Cathode for Ultrafast-Kinetics Zinc-Ion Batteries

Ming Chen,[a,b] Cuihong He,[a] Qin Liu,[a] Wenzhuo Deng, ‡*[a] and Chuan-Fu Sun‡*[a,b]

Part 1: Experimental Procedures and Theoretical Methods

Part 2: Supporting Figures

Part 1: Experimental Procedures and Theoretical Methods

Synthesis of KZVO-MPs and KZVO-NPs

10 mmol $Zn(CH_3COO)_2$ and 10 mmol KVO_3 were dissolved in 50 and 100 mL deionized water, respectively. Subsequently, the KVO_3 solution was added into $Zn(CH_3COO)_2$ solution and the pH value of the mixture was adjusted to approximately 5 with acetic acid. The yielded microscale precipitate (KZVO-MPs) after magnetically stirring for 2 h at room temperature was collected by centrifugation, washing for three times with deionized water, and then drying at 80 °C in air. The nanoparticles (KZVO-NPs) were obtained after ball milling of KZVO-MPs for 50 hours.

The synthesis path of KZVO can be depicted through the following chemical reaction[1, 2]:

$$2K^+ + 2Zn^{2+} + (V_{10}O_{28})^{6-} + nH_2O \rightarrow K_2Zn_2V_{10}O_{28} \cdot nH_2O$$

The pH plays a key role in the preparation of KZVO. The polyvanadate ions survive in the pH range between 2 and 6.5. The chemical equilibria pivotal to this process are as follows:

$$10VO_2{}^+ + 8H_2O \leftrightarrow H_2V_{10}O_{28}{}^{4-} + 14H^+$$

$$H_2V_{10}O_{28}{}^{4-} \leftrightarrow HV_{10}O_{28}{}^{5-} + H^+$$

$$HV_{10}O_{28}{}^{5-} \leftrightarrow V_{10}O_{28}{}^{6-} + H^+$$

By carefully adjusting the concentration of H^+ through the addition of acetic acid, we can successfully make the existence of abundant decavanadate ions possible, which will be instrumental for the subsequent fabrication of the final product KZVO materials.

Material Characterizations

The crystallographic structure of the as-prepared product was identified by the powder X-ray diffractometer (XRD, Ultima IV, Rigaku) with the Cu-Kα radiation. The morphology and elemental mapping of KZVO were characterized by the scanning electron microscopy (SEM, Phenom LE), the energy dispersive spectroscopy (EDS), and the transmission electron microscope (TEM, Tecnai F20). X-ray photoelectron spectroscopy (XPS, ESCALAB 250Xi, Thermo Scientific Instrument) was conducted to analyze the oxidation states. Thermogravimetric analysis (TGA, STA 449F3, Netzsch) was performed at a heating rate of 10 °C min^{-1} under Ar flow. The batteries were disassembled after discharging/charging to certain voltages at different cycles and the cathodes were washed thoroughly with deionized water prior to ex-situ XRD and XPS characterizations.

Fabrication of ZIBs

The 2032 coin-type batteries were fabricated using Zn foil anodes of 10 mm in diameter, aqueous electrolytes of 4 M $Zn(CF_3SO_3)_2$, Whatman glass-fiber separators/NKK cellulose membranes(TF4050), and the KZVO-containing cathodes. The complexed cathode was prepared by rolling the active material, Ketjen Black (KB) conductive agent, and polytetrafluoroethylene(PTFE) binder in a weight ratio of 70: 20: 10 onto a titanium mesh (200 mesh) with a massloading of ~ 2.5 mg cm^{-2}, and then cut into discs with the diameter of 1 cm after drying under vacuum at 80 °C for 12 h.

Electrochemical Measurements

The cyclic voltammetry (CV) experiments were performed using the CHI600E electrochemical workstation at a scan rate of 0.1 mV s^{-1} in a voltage range of 0.2 to 1.8 V. The galvanostatic charge/discharge tests were conducted on the LANHE CT2001 battery testing system within a voltage range of 0.2-1.8 V at a constant temperature of 28 °C. Linear-scan CV measurements and electrochemical impedance spectroscopy (EIS) were carried out on the Bio-Logic SP-300 electrochemical workstation. The galvanostatic intermittent titration technique (GITT) was performed using the LANHE CT2001 battery testing instrument, current pulses of 30 minutes at a rate of 20 mA g^{-1} followed by a three-hour rest step were applied and the process was repeated until the cell voltage reached 0.2 V/1.8 V. Prior to the GITT test, the batteries were activated through eight cycles of galvanostatic cycling at 20 mA g^{-1} within the voltage range of 0.2-1.8 V. The Zn^{2+}-ion diffusion coefficients were calculated by the following equation[3]:

$$D_{Zn^{2+}} = \frac{4}{\tau\pi}\left(\frac{n_M V_M}{S}\right)^2\left(\frac{\Delta E_s}{\Delta E_t}\right)^2$$

where τ is the constant current pulse duration; V_M represents the mole volume of active materials, n_M refers to the mole number of active materials, S is the effective contact area of active materials (herein, geometry area is adopted for estimation), ΔE_s and ΔE_t represent the change in steady-state voltage and overall cell voltage, respectively, when a current pulse is applied during a single step GITT experiment.

DFT calculations

The initial structural model $Zn_2V_5O_{14}{\cdot}4H_2O$ was created by substituting Zn for K in $KZnV_5O_{14}{\cdot}8H_2O$ (ICSD# 94840). We employed density functional theory (DFT) to fully relax the produced configuration. The projector-augmented wave (PAW) pseudopotentials[4] was adopted to describe the ionic shell, and the Perdew, Burke, and Ernzerhof (PBE)[5] functional of general gradient approximation (GGA) was applied to account for the exchange and correlation interactions of the valence electrons. We used a plane wave energy cutoff of 520 eV and a Γ-centered Monkhorst-Pack k-grid 4 x 3 x 5 to integrate the Brillouin zones (BZ). D3 scheme proposed by Grimme[6] was utilized to take the dispersion interactions into consideration. A Hubbard U value of 3.25 eV[7] was selected to account for the on-site repulsion of the localized V 3d electrons. The convergence criteria for the energy difference between each electronic iteration and the force exerted on each atom are 1×10^{-6} eV and 0.03 eV/Å, respectively. We searched the transition state using the climbing image-nudged elastic band (CI-NEB) method. Initial six images between the endmembers were generated using the atomic simulation environment (ASE)[8], and a saddle point was obtained until the energy and force were converged to 1×10^{-6} eV and 0.05 eV/Å, respectively. All the spin-polarized computations were conducted using the Vienna ab initio simulation package (VASP)[9].

Part 2: Supporting Figures

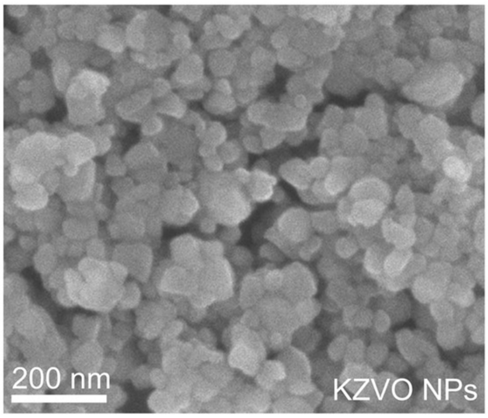

Figure S1. SEM images of KZVO NPs.

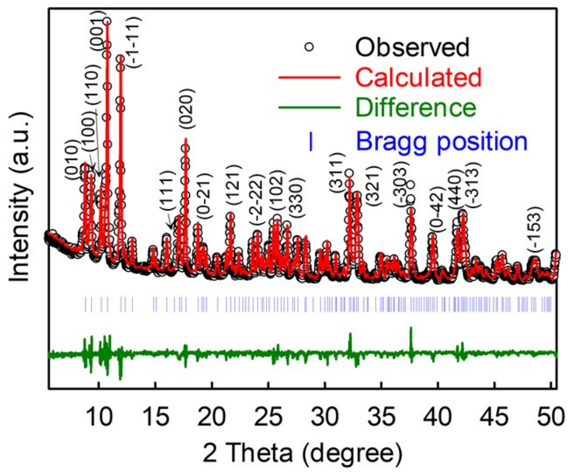

Figure S2. XRD and Rietveld refinement of KZVO-MPs (Rwp=10.59%, Rp=8.00%).

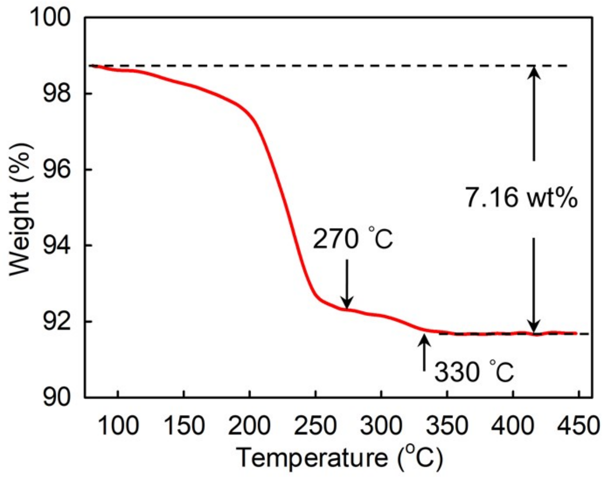

Figure S3. Thermogravimetric analysis of KVP-NPs.

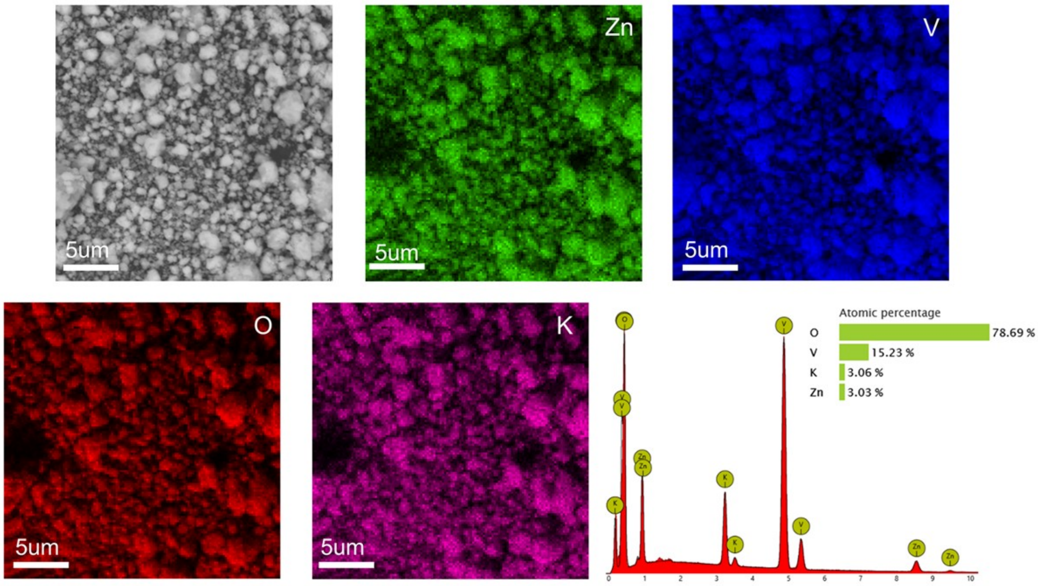

Figure S4. SEM and EDS results for KZVO-MPs, and the obtained atomic ratio of K, Zn and V is 1:1:5.02.

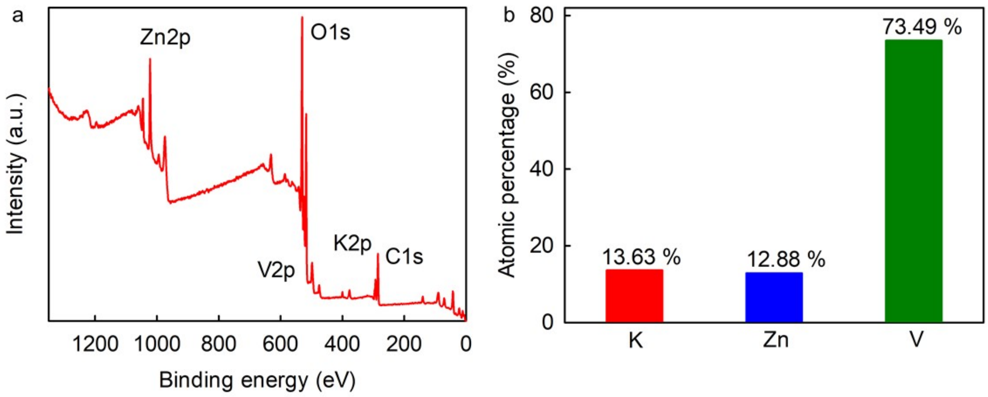

Figure S5. (a) The XPS survey spectrum and (b) the derived atomic percentage of K, Zn and V.

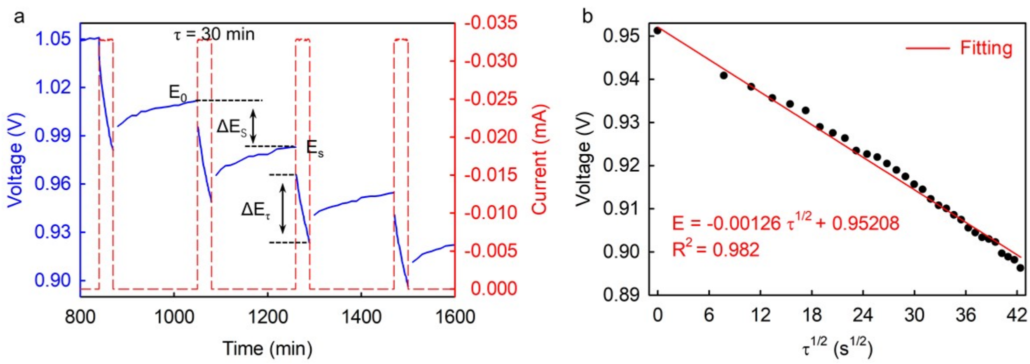

Figure S6 (a) Voltage (V) *vs*. time (t) profile of the ZVO cathode during GITT measurement. (b) The linear behavior of the transient voltage changes E vs. $\tau^{1/2}$ during the discharge.

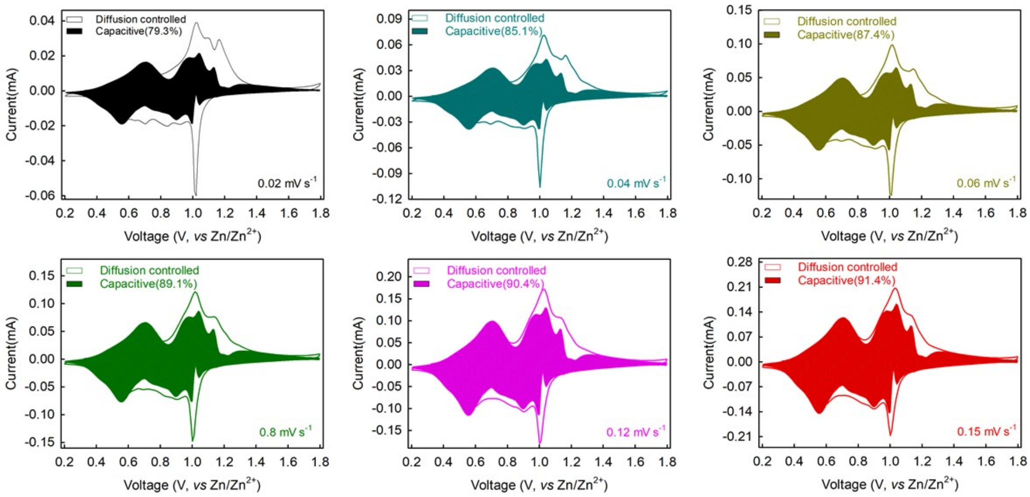

Figure S7 Capacity contribution analysis at scan rates of 0.02, 0.04, 0.06, 0.08, 0.12, 0.15 mV s^{-1}.

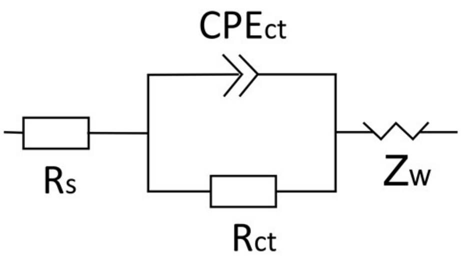

Figure S8. equivalent circuit of EIS.

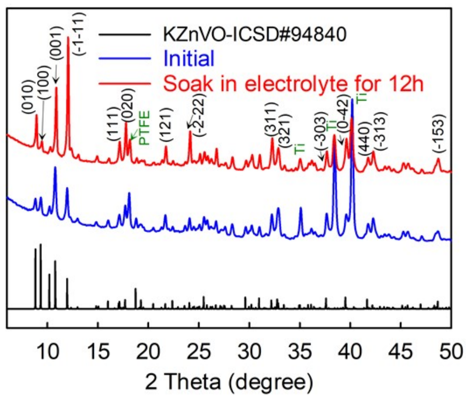

Figure S9. XRD patterns of the KZVO electrode at the initial state and after soaking for 12 h.

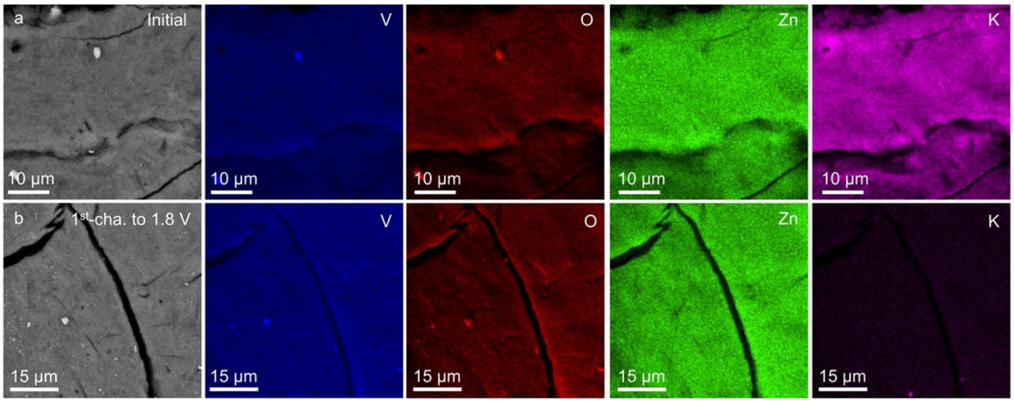

Figure S10. SEM and EDS mapping of the electrode at the initial state and after charging to 1.8 V.

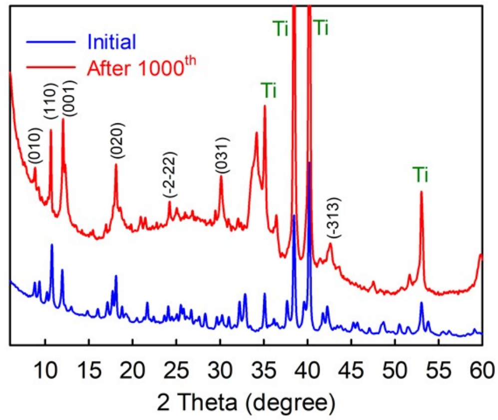

Figure S11. XRD patterns of the KZVO electrode at the initial state and full charge state after 1000 cycles at the current of 1 A g^{-1}.

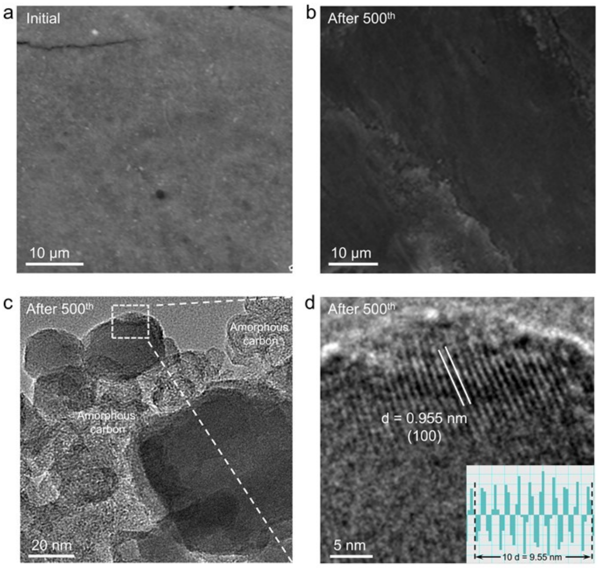

Figure S12. (a) SEM images of KZVO electrode at initial state. (b) SEM images of KZVO electrode after 500 cycles at 1 A g^{-1}. (c-d) TEM and HRTEM images of KZVO electrode after 500 cycles at 1 A g^{-1}.

Table S1. Comparison of cycling stability and specific capacities.

Ref.	**Cathode**	**Specific capacity (mAh g-1)@ current (A g-1)**	**Current (A g-1)/C-rate**	**Cycle number (n)/Cycle time(days)**	**Retention (%)**
	This work	275@0.02	0.3/1.2C	400/25	~80.8
10	$Na_6[V_{10}O_{28}]$ $2.6H_2O$	228.5@0.1	0.3/~1.31C	100/~1.3	~85.6
11	$K_{1.1}V_3O_8$	386@0.1	0.2/~1.2C	50/~7.5	~91.35
11	$Na_{1.16}V_3O_8$	266.9@0.1	0.2/~0.75C	50/~4.5	~78.8
12	$Ag_{0.4}V_2O_5$	367@0.1	0.5/~1.36C	50/~2.1	~78.8
13	$Na_{1.1}V_3O_{7.9}$@rGO	240@0.05	0.3/~1.25C	100/~5.5	~74.8
14	$Zn_3V_2O_7(OH)_2{\cdot}2H_2O$	213@0.05	0.2/~0.94C	300/~13.9	~63.8
15	$Ba_{1.2}V_6O_{16}{\cdot}3H_2O$	345.5@0.1	0.5/~1.44C	200/~7	~75.9
16	$Zn_2V_2O_7$	248@0.05	0.3/~1.2C	200/~11.8	~86
17	V_6O_{13}	360@0.2	0.4/~1.1C	200/~13.7	~80
18	$KV_2O_4PO_4{\cdot}3.2H_2O$	226@0.02	0.2/~0.88C	100/~16.1	~83
19	$ZnV_6O_{16}{\cdot}8H_2O$	365@0.5	0.5/~1.37C	300/~17.3	~86

20	$LiV_2(PO_4)_3$	198@0.136	0.136/~1C	200/~18.8	~86
21	$NH_4V_4O_{10}$	147@0.05	0.2/~1.36C	200/~10.2	~97.6
22	Mn_3O_4	239.2@0.1	0.2/~0.84C	70/~4.6	~64.7
23	$Cu[Fe(CN)_6]_{2/3}\cdot nH_2O$	60@0.06	0.06/~1C	60/~5	~90.9
24	ZnHCFs	65.4@0.06	0.06/~1C	100/~8	~76
25	$K_2MnFe(CN)_6$	138@0.2	0.2/~1.45C	400/~17.3	~72.5

Table S2. Comparison of the rate performance.

Ref.	Cathode	Rate performance
	This work	capacities of 262, 255, 247, 238, 228, 220, 212, 207, 200, 191, 186, 180, 167, 160 and 150 mAh g^{-1} at current densities of 0.02, 0.05, 0.1, 0.2, 0.5, 1, 2, 3, 5, 8, 10, 12, 15, 18 and 20 A g^{-1}, respectively.
26	V_2O_5	capacities of 242, 217, 192, 171, and 156 mAh g^{-1} at current densities of 0.05, 0.1, 0.2, 0.5, and 1 A g^{-1}, respectively.
27	$Mg_xV_2O_5 \cdot nH_2O$	capacities of 353, 330, 291, 264, 221, 167 and 81 mAh g^{-1} at current densities of 0.05, 0.1, 0.5, 1, 2, 3, and 5 A g^{-1}, respectively.
28	$KV_3O_8 \cdot 0.75H_2O$	capacities of 381, 375, 310, 290, 250, and 206 mAh g^{-1} at current densities of 0.1, 0.2, 0.5, 1, 2, and 5 A g^{-1}, respectively.
29	$Zn_{0.1}V_2O_5 \cdot nH_2O$	capacities of 450, 422, 408, 362, 317, and 280 mAh g^{-1} at current densities of 0.3, 0.6, 1, 2, 4, and 6 A g^{-1}, respectively.
30	$V_5O_{12} \cdot 6H_2O$	capacities of 467, 439, 404, 381, 365, 337, 297 and 263 mAh g^{-1} at current densities of 0.1, 0.2, 0.5, 1, 2, 5, 10 and 20 A g^{-1}, respectively.
31	$NaCa_{0.6}V_6O_{16} \cdot 3H_2O$	capacities of 347, 310, 279, 243, 202, and 154 mAh g^{-1} at current densities of 0.1, 0.3, 0.6, 1.2, 2.4, and 5 A g^{-1}, respectively.
32	$Mn_{0.15}V_2O_5 \cdot nH_2O$	capacities of 299, 268, 238, 222, 193, and 150 mAh g^{-1} at current densities of 0.5, 1, 2, 3, 5, and 10 A g^{-1}, respectively.
33	$Co_{0.247}V_2O_5$ $0.944H_2O$	capacities of 421, 380, 323, 260, 223, 184, 176, 165 and 163 mAh g^{-1} at current densities of 0.1, 0.3, 0.5, 1, 2, 4, 6, 8 and 10 A g^{-1}, respectively.
34	Mg^{2+} doping $NH_4V_4O_{10}$	capacities of 410, 368, 338, 306, 253, 200, 165, and 140 mAh g^{-1} at current densities of 0.1, 0.5, 1, 2, 5, 10, 15 and 20 A g^{-1}, respectively.
10	$Na_6[V_{10}O_{28}]$ nH_2O	capacities of 228.5, 191, 151.7, 129.7, 112.7, 96.7, and 86.4 mAh g^{-1} at current densities of 0.1, 0.2, 0.5, 1, 2, 5 and 10 A g^{-1}, respectively.
11	$K_{1.1}V_3O_8$	capacities of 349, 308, 280, 253, 214 and 184 mAh g^{-1} at current densities of 0.2, 0.5, 1, 2, 5, and 10 A g^{-1}, respectively.
12	$Ag_{0.4}V_2O_5$	capacities of 353, 282, 253, 218 and 186 mAh g^{-1} at current densities of 0.1, 0.3, 0.5, 1 and 2 A g^{-1}, respectively.
35	$Na_2V_6O_{16} \cdot 3H_2O$	capacities of 361, 341, 319, 301, 277, 230 174 and 114 mAh g^{-1} at current densities of 0.1, 0.5, 1, 1.5, 3, 6, 9, and 20 A g^{-1},respectivel.
36	$K_2Zn_2V_{10}O_{28}$	capacities of 225.7, 200.8, 161.2, 126.4, 100.8 and 71.7 mAh g^{-1} at current densities of 0.05, 0.1, 0.2, 0.5, 1, and 2 A g^{-1}, respectively.
37	NaV_3O_8	capacities of 400, 303, 270, 231,166 and 105 mAh g^{-1} at current densities of 0.1, 0.5, 1, 2, 5 and 10 A g^{-1}, respectively.

38	$Na_5V_{12}O_{32}$	capacities of 290.6, 244.5, 199, 121.3 and 59.7 mAh g^{-1} at current densities of 0.3, 0.5, 1, 2 and 5 A g^{-1}, respectively.
38	$HNaV_6O_{16}\cdot4H_2O$	capacities of 362, 296, 208, 141 and 78 mAh g^{-1} at current densities of 0.3, 0.5, 1, 2 and 5 A g^{-1}, respectively.
39	$K_{10}[V^{IV}{}_{16}V^{V}{}_{18}O_{82}]$	capacities of 397, 383, 358, 335, 313, 285, 268, 243, 220, 175 and 133 mAh g^{-1} at current densities of 0.05, 0.1, 0.2, 0.5, 1, 2, 3, 4, 5, 7 and 9 A g^{-1}, respectively.
14	$Zn_3V_2O_7(OH)_2\cdot2H_2O$	capacities of 200, 166, 145, 122, 105, 84, 75 and 54 mAh g^{-1} at current densities of 0.05, 0.1, 0.3, 0.5, 0.8, 1, 2 and 3 A g^{-1}, respectively.
15	$Ba_{1.2}V_6O_{16}\cdot3H_2O$	capacities of 321, 277, 247, 223, 198, 168, 151, 130 and 109 mAh g^{-1} at current densities of 0.1, 0.2, 0.3, 0.5, 1, 2, 3, 5 and 10 A g^{-1}, respectively.
40	$(NH4)_{0.5}V_2O_5$	capacities of 395, 259, 333, 305, 252, 204 and 154 mAh g^{-1} at current densities of 0.2, 0.5, 1, 2, 5, 10 and 20 A g^{-1}, respectively.
41	$Na_3V_2(PO_4)_3$/Go	capacities of 107, 102, 99, 96, 88 and 82 mAh g^{-1} at current densities of 0.05, 0.1, 0.2, 0.5, 1 and 2 A g^{-1}, respectively.
42	$H_2V_3O_8$	capacities of 410.3, 297.4, 240.5, 155 and 113.9 mAh g^{-1} at current densities of 0.1, 0.5, 1, 3 and 5 A g^{-1}, respectively.
43	$Zn_3V_3O_8$	capacities of 232, 213, 194, 173, 160, 150 and 141 mAh g^{-1} at current densities of 0.2, 0.5, 1, 2, 3, 4 and 5 A g^{-1}, respectively.
16	$Zn_2V_2O_7$	capacities of 250, 248, 231, 223, 248, 213, 209, 205, 190 and 170 mAh g^{-1} at current densities of 0.05, 0.1, 0.2, 0.3, 0.5, 0.7,0.9, 1.1, 2.2 and 4.4 A g^{-1}, respectively.
44	$Na_3V_2(PO_4)_3$	capacities of 97, 89, 79 and 58 mAh g^{-1} at current densities of 0.05, 0.1, 0.5 and 1 A g^{-1}, respectively.
45	V_2O_5 $2.2H_2O$	capacities of 451, 430, 407, 384, 362, 300 and 224 mAh g^{-1} at current densities of 0.1, 0.2, 0.5, 1, 2, 5 and 10 A g^{-1}, respectively.
46	$Ca_{0.67}V_8O_{20}\cdot3.5H_2O$	capacities of 466, 403, 373, 336, and 313 mAh g^{-1} at current densities of 0.1, 0.4, 0.8, 1.6 and 2.4 A g^{-1}, respectively.
18	$KV_2O_4PO_4\cdot3.2H_2O$	capacities of 226, 223, 219, 210, 195, 181, 172, 167, 160, 152 and 135 mAh g^{-1} at current densities of 0.02, 0.05, 0.1, 0.2, 0.5, 1, 2, 3, 5, 7 and 9 A g^{-1}, respectively.
47	$Na_{0.33}V_2O_5$	capacities of 367, 252, 173, 145, 137 and 96 mAh g^{-1} at current densities of 0.1, 0.2, 0.5, 0.8, 1 and 2 A g^{-1}, respectively.
19	$ZnV_6O_{16}\cdot8H_2O$	capacities of 400, 355, 328, 295, 238, 198 and 167 mAh g^{-1} at current densities of 0.3, 0.6, 1, 2, 5, 10 and 15 A g^{-1}, respectively.
48	$CaV_6O_{16}\cdot3H_2O$	capacities of 286, 260, 235, 202, 153, 115 and 78 mAh g^{-1} at current densities of 0.2, 0.5, 1, 2, 5, 10 and 20 A g^{-1}, respectively.
21	$NH_4V_4O_{10}$	capacities of 147, 137, 127, 118, 105, 98, 91, 80 and 72 mAh g^{-1} at current

		densities of 0.05, 0.1, 0.2, 0.3, 0.6, 0.8, 1, 1.5 and 2 A g^{-1}, respectively.
49	$Zn_{0.3}V_2O_5 \cdot 1.5H_2O$	capacities of 426, 400, 389, 369, 335 and 265 mAh g^{-1} at current densities of 0.2, 0.5, 1, 2, 5 and 10 A g^{-1}, respectively.
50	$KV_5O_{13} \cdot nH_2O$	capacities of 444, 428, 411, 388, 370, 357, 336, 323 and 313 mAh g^{-1} at current densities of 0.5, 0.5, 1, 2, 3, 4, 6, 8 and 10 A g^{-1}, respectively.
51	$Zn_{0.25}V_2O_5 \cdot nH_2O$	capacities of 300, 278, 270, 260, 260, and 250 mAh g^{-1} at current densities of 0.05, 0.3, 0.6, 1.2, 2.4, and 3 A g^{-1}, respectively.
52	$Li_xV_2O_5 \cdot nH_2O$	capacities of 470, 386, 316, 236, 190 and 170 mAh g^{-1} at current densities of 0.5, 1, 2, 5, 8 and 10 A g^{-1}, respectively.
53	$Ca_{0.25}V_2O_5 \cdot nH_2O$	capacities of 340, 289, 260, 250, 220 and 200 mAh g^{-1} at current densities of 0.05, 0.3, 0.6, 0.9, 1.4 and 2.9 A g^{-1}, respectively.
17	V_6O_{13}	capacities of 370, 333, 275, 252, 205 and 142mAh g^{-1} at current densities of 0.2, 0.4, 4, 6, 12 and 24 A g^{-1}, respectively.
54	CuV_2O_6	capacities of 361, 316, 285, 256 and 217 mAh g^{-1} at current densities of 0.2, 0.5, 1, 2 and 5 A g^{-1}, respectively.
55	$V_3O_7 \cdot nH_2O$	capacities of 481.8, 450.2, 404.7, 352.9, 280.6 and 162.5 mAh g^{-1} at current densities of 0.1, 0.2, 0.5, 1, 2 and 5 A g^{-1}, respectively.
56	$K_2V_8O_{21}$	capacities of 247, 226, 183, 139 and 92 mAh g^{-1} at current densities of 0.3, 0.4, 1, 2 and 4 A g^{-1}, respectively.
57	$K_{0.5}V_2O_5$	capacities of 486, 461, 427, 398, 352 and 256 mAh g^{-1} at current densities of 0.1, 0.2, 0.5, 1, 2 and 5 A g^{-1}, respectively.
58	$K_4Na_2V_{10}O_{28}$	capacities of 127.6, 120.3, 106.3, 91.4, 85.8 and 84.4 mAh g^{-1} at current densities of 0.05, 0.1, 0.2, 0.5, 0.8 and 1 A g^{-1}, respectively.
59	Mn_3O_4@C	capacities of 323.2, 270.1, 209.6, 130.5 and 102.3 mAh g^{-1} at current densities of 0.1, 0.2, 0.5, 1 and 2 A g^{-1}, respectively.
60	δ-MnO_2	capacities of 232, 187, 161, 145, 134, 125, 111 and 103 mAh g^{-1} at current densities of 0.76, 1.52, 2.28, 3.04, 3.8, 4.56, 6.08 and 7.6 A g^{-1}, respectively.
61	MnO	capacities of 267, 247, 216, 172, 126 and 95 mAh g^{-1} at current densities of 0.1, 0.2, 0.4, 0.6, 0.8 and 1 A g^{-1}, respectively.
62	$ZnMn_2O_4$	capacities of 127, 132, 129, 118, 98, 83 and 70 mAh g^{-1} at current densities of 1, 0.2, 0.4, 0.8,1.6, 2.4 and 3.2 A g^{-1}, respectively.
24	ZnHCF	capacities of 65.4, 60.4, 56.8, 52.5, 45.5, 39.1 and 32.3 mAh g^{-1} at current densities of 0.06, 0.12, 0.18, 0.3, 0.6, 0.9 and 1.2 A g^{-1}, respectively.
63	β-MnO_2	capacities of 312, 247, 193, 157, 123 and 86 mAh g^{-1} at current densities of 0.03, 0.06, 0.13, 0.26, 0.53 and 1.06 A g^{-1}, respectively.
64	α-MnO_2	capacities of 323, 273, 231, 197, 163, 120, 79 and 47 mAh g^{-1} at current densities of 0.016, 0.033, 0.066, 0.133, 0.266, 0.533, 1.066 and 1.666 A g^{-1}, respectively.

Table S3. Comparison of the Zn^{2+}-ion migration energy barriers.

Ref.	Cathode materials	energy barrier (eV)
-	This work	0.58
65	MgV_2O_6 1.7H_2O	0.896
65	$Mg_{0.55}V_2O_5$ 0.8H_2O	1.16
66	V_2O_5 1.75H_2O	0.81
67	VO_2	0.78
31	$NaCa_{0.6}V_6O_{16}$ 3H_2O	0.53
17	V_6O_{13}	0.87
11	$Li_{1.2}V_3O_8$	0.64
11	$Na_{1.16}V_3O_8$	0.64
68	(Na,Mn)V_8O_{20}·nH2O	0.72
17	V_6O_{13} nH_2O	0.87

Table S4. The SEM-EDS mapping at different state

Area	Initial			1^{st}-dis.0.2V			1^{st}-cha.1.8V			2^{nd}-dis.0.2V			2^{nd}-cha.1.8V		
	K	Zn	V	K	Zn	V	K	Zn	V	K	Zn	V	K	Zn	V
1	1	1.04	5	0.38	3.8	5	0	1.76	5	0.02	3.76	5	0	1.89	5
2	0.99	1.04	5	0.39	3.64	5	0.02	1.78	5	0	3.85	5	0	1.84	5
3	0.97	0.98	5	0.47	3.66	5	0	1.85	5	0.02	3.89	5	0	1.93	5
4	0.99	1.03	5	0.41	3.42	5	0	1.75	5	0	3.74	5	0	1.96	5
5	1.01	1.07	5	0.38	3.67	5	0.01	1.86	5	0.02	3.86	5	0	2.02	5
average	1	1	5	0.4	3.6	5	0	1.8	5	0	3.8	5	0	1.9	5

References

1. J. Howard T. Evans, The Molecular Structure of the Isopoly Complex Ion, Decavanadate ($V_{10}O_{28}^{6-}$), *Inorg. Chem.*, 1966, **5**, 967-977.
2. O. V. Yakubovich, E. N. Anan'eva and O. V. Dimitrova, Refinement of the Crystal Structure of $K_2Zn_2V_{10}O_{28}\cdot16H_2O$, *Doklady Physics*, 2002, **47**, 346-352.
3. W. Weppner and R. A. Huggins, Determination of the Kinetic Parameters of Mixed-Conducting Electrodes and Application to the System Li_3Sb, *J. Electrochem. Soc.*, 1977, **124**, 1569-1577.
4. G. Kresse and D. Joubert, From ultrasoft pseudopotentials to the projector augmented-wave method, *Physical Review B*, 1999, **59**, 1758-1775.
5. J. P. Perdew, K. Burke and M. Ernzerhof, Generalized gradient approximation made simple, *Phys. Rev. Lett.*, 1996, **77**, 3865-3868.
6. S. Grimme, J. Antony, S. Ehrlich and H. Krieg, A consistent and accurate ab initio parametrization of density functional dispersion correction (DFT-dD) for the 94 elements H-Pu, *J. Chem. Phys.*, 2010, **132**, 154104.
7. N. J. Szymanski, Z. T. Y. Liu, T. Alderson, N. J. Podraza, P. Sarin and S. V. Khare, Electronic and Optical Properties of Vanadium Oxides from First Principles, *Comput.Mater.Sci.*, 2018, **146**, 310-318.
8. A. Hjorth Larsen, J. Jørgen Mortensen, J. Blomqvist, I. E. Castelli, R. Christensen, M. Dułak, J. Friis, M. N. Groves, B. Hammer, C. Hargus, E. D. Hermes, P. C. Jennings, P. Bjerre Jensen, J. Kermode, J. R. Kitchin, E. Leonhard Kolsbjerg, J. Kubal, K. Kaasbjerg, S. Lysgaard, J. Bergmann Maronsson, T. Maxson, T. Olsen, L. Pastewka, A. Peterson, C. Rostgaard, J. Schiøtz, O. Schütt, M. Strange, K. S. Thygesen, T. Vegge, L. Vilhelmsen, M. Walter, Z. Zeng and K. W. Jacobsen, The AtomicSimulation Environment-A Python Library for Working with Atoms, *J. Phys. Condens. Matter*, 2017, **29**, 273002.
9. G. Kresse and J. Furthmuller, Efficient iterative schemes for ab initio total-energy calculations

using a plane-wave basis set, *Physical Review B*, 1996, **54**, 11169-11186.
10. H. He, F.-C. Pan, X.-W. Liang, Q. Hu, S. Liu, J. Hu, S. C. Jun, D. Lin, Y. Yamauchi and Y. Huo, Unveiling the Effect of Structural Water on Zn-ionStorage of Polyoxovanadate for High-Rate and Long-life Aqueous Zinc Ion Battery, *Chem. Eng. J.*, 2023, **462**, 142221.
11. G. Zhang, T. Wu, H. Zhou, H. Jin, K. Liu, Y. Luo, H. Jiang, K. Huang, L. Huang and J. Zhou, Rich Alkali Ions Preintercalated Vanadium Oxides for Durable and Fast Zinc-Ion Storage, *ACS Energy Lett.*, 2021, **6**, 2111-2120.
12. L. Shan, Y. Yang, W. Zhang, H. Chen, G. Fang, J. Zhou and S. Liang, Observation of Combination Displacement/Intercalation Reaction in Aqueous Zinc-Ion Battery, *Energy Stor. Mater.*, 2019, **18**, 10-14.
13. Y. Cai, F. Liu, Z. Luo, G. Fang, J. Zhou, A. Pan and S. Liang, Pilotaxitic $Na_{1.1}V_3O_{7.9}$ Nanoribbons/Graphene as High-Performance Sodium Ion Battery and Aqueous Zinc Ion Battery Cathode, *Energy Stor. Mater.*, 2018, **13**, 168-174.
14. C. Xia, J. Guo, Y. Lei, H. Liang, C. Zhao and H. N. Alshareef, Rechargeable Aqueous Zinc-Ion Battery Based on Porous Framework Zinc Pyrovanadate Intercalation Cathode, *Adv. Mater.*, 2018, **30**, 1705580.
15. X. Wang, B. Xi, X. Ma, Z. Feng, Y. Jia, J. Feng, Y. Qian and S. Xiong, Boosting Zinc-Ion Storage Capability by Effectively Suppressing Vanadium Dissolution Based on Robust Layered Barium Vanadate, *Nano Lett.*, 2020, **20**, 2899-2906.
16. B. Sambandam, V. Soundharrajan, S. Kim, M. H. Alfaruqi, J. Jo, S. Kim, V. Mathew, Y.-k. Sun and J. Kim, Aqueous Rechargeable Zn-Ion Batteries: An Imperishable and High-Energy $Zn_2V_2O_7$ Nanowire Cathode Through Intercalation Regulation, *J. Mater. Chem. A.*, 2018, **6**, 3850-3856.
17. J. Shin, D. S. Choi, H. J. Lee, Y. Jung and J. W. Choi, Hydrated Intercalation for High-Performance Aqueous Zinc Ion Batteries, *Adv. Energy Mater.*, 2019, **9**, 1900083.
18. X. Yang, W. Deng, M. Chen, Y. Wang and C. F. Sun, Mass-Producible, Quasi-Zero-Strain, Lattice-Water-Rich Inorganic Open-Frameworks for Ultrafast-Charging and Long-Cycling Zinc-Ion Batteries, *Adv. Mater.*, 2020, **32**, 2003592
19. K. Zhu, W. Jiang, Z. Wang, W. Li, W. Xie, H. Yang and W. Yang, Hewettite $ZnV_6O_{16} \cdot 8H_2O$ with Remarkably Stable Layers and Ultralarge Interlayer Spacing for High-Performance Aqueous Zn-Ion Batteries, *Angew. Chem. Int. Ed.*, 2023, **62**, e202213368.
20. C. Li, R. Kingsbury, L. Zhou, A. Shyamsunder, K. A. Persson and L. F. Nazar, Tuning the Solvation Structure in Aqueous Zinc Batteries to Maximize Zn-Ion Intercalation and Optimize Dendrite-Free Zinc Plating, *ACS Energy Lett.*, 2022, **7**, 533-540.
21. G. Yang, T. Wei and C. Wang, Self-Healing Lamellar Structure Boosts Highly Stable Zinc-Storage Property of Bilayered Vanadium Oxides, *ACS Appl. Mater. Interfaces*, 2018, **10**, 35079-35089.
22. J. Hao, J. Mou, J. Zhang, L. Dong, W. Liu, C. Xu and F. Kang, Electrochemically Induced Spinel-Layered Phase Transition of Mn_3O_4 in High Performance Neutral Aqueous Rechargeable Zinc Battery, *Electrochim. Acta*, 2018, **259**, 170-178.
23. V. Renman, D. O. Ojwang, M. Valvo, C. P. Gómez, T. Gustafsson and G. Svensson, Structural-Electrochemical Relations in the Aqueous Copper Hexacyanoferrate-Zinc System Examined by Synchrotron X-ray Diffraction, *J. Power Sources*, 2017, **369**, 146-153.
24. L. Zhang, L. Chen, X. Zhou and Z. Liu, Towards High-Voltage Aqueous Metal-Ion Batteries Beyond 1.5 V: The Zinc/Zinc Hexacyanoferrate System, *Adv. Energy Mater.*, 2015, **5**, 1400930.
25. W. Deng, Z. Li, Y. Ye, Z. Zhou, Y. Li, M. Zhang, X. Yuan, J. Hu, W. Zhao, Z. Huang, C. Li, H. Chen, J.

Zheng and R. Li, Zn^{2+}Induced Phase Transformation of $K_2MnFe(CN)_6$ Boosts Highly Stable Zinc-Ion Storage, *Adv. Energy Mater.*, 2021, **11**, 2003639.
26. P. Hu, M. Yan, T. Zhu, X. Wang, X. Wei, J. Li, L. Zhou, Z. Li, L. Chen and L. Mai, Zn/V_2O_5 Aqueous Hybrid-Ion Battery with High Voltage Platform and Long Cycle Life, *ACS Appl. Mater. Interfaces*, 2017, **9**, 42717-42722.
27. F. Ming, H. Liang, Y. Lei, S. Kandambeth, M. Eddaoudi and H. N. Alshareef, Layered $Mg_xV_2O_5 \cdot nH_2O$ as Cathode Material for High-Performance Aqueous Zinc Ion Batteries, *ACS Energy Lett.*, 2018, **3**, 2602-2609.
28. F. Wan, S. Huang, H. Cao and Z. Niu, Freestanding Potassium Vanadate/Carbon Nanotube Films for Ultralong-Life Aqueous Zinc-Ion Batteries, *ACS Nano*, 2020, **14**, 6752-6760.
29. K. Zhu, T. Wu, W. van den Bergh, M. Stefik and K. Huang, Reversible Molecular and Ionic Storage Mechanisms in High-Performance $Zn_{0.1}V_2O_5.nH_2O$ Xerogel Cathode for Aqueous Zn-Ion Batteries, *ACS Nano*, 2021, **15**, 10678-10688.
30. T. Wei, Q. Li, G. Yang and C. Wang, Pseudo-Zn-Air and Zn-Ion Intercalation Dual Mechanisms to Realize High-Areal Capacitance and Long-Life Energy Storage in Aqueous Zn Battery, *Adv. Energy Mater.*, 2019, **9**, 1901480.
31. K. Zhu, T. Wu and K. Huang, $NaCa_{0.6}V_6O_{16}.3H_2O$ as An Ultra-Stable Cathode for Zn-Ion Batteries: The Roles of Pre-Inserted Dual-Cations and Structural Water in V_3O_8 Layer, *Adv. Energy Mater.*, 2019, **9**, 1901968.
32. H. Geng, M. Cheng, B. Wang, Y. Yang, Y. Zhang and C. C. Li, Electronic Structure Regulation of Layered Vanadium Oxide via Interlayer Doping Strategy toward Superior High-Rate and Low-Temperature Zinc-Ion Batteries, *Adv. Funct. Mater.*, 2019, **30**, 1907684.
33. L. T. Ma, N. Li, C. B. Long, B. B. Dong, D. L. Fang, Z. X. Liu, Y. W. Zhao, X. L. Li, J. Fan, S. M. Chen, S. J. Zhang and C. Y. Zhi, Achieving Both High Voltage and High Capacity in Aqueous Zinc-Ion Battery for Record High Energy Density, *Adv. Funct. Mater.*, 2019, **29**, 1906142.
34. X. Wang, Y. Wang, A. Naveed, G. Li, H. Zhang, Y. Zhou, A. Dou, M. Su, Y. Liu, R. Guo and C. C. Li, Magnesium Ion Doping and Micro-Structural Engineering Assist $NH_4V_4O_{10}$ as a High-Performance Aqueous Zinc Ion Battery Cathode, *Adv. Funct. Mater.*, 2023, **33**, 2306205.
35. V. Soundharrajan, B. Sambandam, S. Kim, M. H. Alfaruqi, D. Y. Putro, J. Jo, S. Kim, V. Mathew, Y. K. Sun and J. Kim, $Na_2V_6O_{16}$ $3H_2O$ Barnesite Nanorod: An Open Door to Display a Stable and High Energy for Aqueous Rechargeable Zn-Ion Batteries as Cathodes, *Nano Lett.*, 2018, **18**, 2402-2410.
36. T. Zhou, L. Zhu, L. Xie, Q. Han, X. Yang, X. Cao and J. Ma, New Insight on $K_2Zn_2V_{10}O_{28}$ as an Advanced Cathode for Rechargeable Aqueous Zinc-Ion Batteries, *Small*, 2022, **18**, 2107102.
37. F. Hu, D. Xie, F. Cui, D. Zhang and G. Song, Synthesis and Electrochemical Performance of NaV_3O_8 Nanobelts for Li/Na-Ion Batteries and Aqueous Zinc-Ion Batteries, *RSC Adv.*, 2019, **9**, 20549-20556.
38. X. Guo, G. Fang, W. Zhang, J. Zhou, L. Shan, L. Wang, C. Wang, T. Lin, Y. Tang and S. Liang, Mechanistic Insights of Zn^{2+} Storage in Sodium Vanadates, *Adv. Energy Mater.*, 2018, **8**, 1801819.
39. K. Yang, Y. Hu, L. Li, L. Cui, L. He, S. Wang, J. Zhao and Y.-F. Song, First High-Nuclearity Mixed-Valence Polyoxometalate with Hierarchical Interconnected Zn^{2+} Migration Channels as an Advanced Cathode Material in Aqueous Zinc-Ion Battery, *Nano Energy*, 2020, **74**, 104851.
40. D. Bin, Y. Liu, B. Yang, J. Huang, X. Dong, X. Zhang, Y. Wang and Y. Xia, Engineering a High-

Energy-Density and Long Lifespan Aqueous Zinc Battery via Ammonium Vanadium Bronze, *ACS Appl. Mater. Interfaces*, 2019, **11**, 20796-20803.

41. P. Hu, T. Zhu, X. Wang, X. Zhou, X. Wei, X. Yao, W. Luo, C. Shi, K. A. Owusu, L. Zhou and L. Mai, Aqueous $Zn//Zn(CF_3SO_3)_2//Na_3V_2(PO_4)_3$ Batteries with Simultaneous Zn^{2+}/Na^+ Intercalation/De-intercalation, *Nano Energy*, 2019, **58**, 492-498.
42. P. He, Y. Quan, X. Xu, M. Yan, W. Yang, Q. An, L. He and L. Mai, High-Performance Aqueous Zinc-Ion Battery Based on Layered $H_2V_3O_8$ Nanowire Cathode, *Small*, 2017, **13**, 1702551.
43. J. Wu, Q. Kuang, K. Zhang, J. Feng, C. Huang, J. Li, Q. Fan, Y. Dong and Y. Zhao, Spinel $Zn_3V_3O_8$: A High-Capacity Zinc Supplied Cathode for Aqueous Zn-Ion Batteries, *Energy Stor. Mater.*, 2021, **41**, 297-309.
44. G. Li, Z. Yang, Y. Jiang, C. Jin, W. Huang, X. Ding and Y. Huang, Towards Polyvalent Ion Batteries: A Zinc-Ion Battery Based on NASICON Structured $Na_3V_2(PO_4)_3$, *Nano Energy*, 2016, **25**, 211-217.
45. J. Zhao, H. Ren, Q. Liang, D. Yuan, S. Xi, C. Wu, W. Manalastas, J. Ma, W. Fang, Y. Zheng, C.-F. Du, M. Srinivasan and Q. Yan, High-Performance Flexible Quasi-Solid-State Zinc-Ion Batteries with Layer-Expanded Vanadium Oxide Cathode and Zinc/Stainless Steel Mesh Composite Anode, *Nano Energy*, 2019, **62**, 94-102.
46. K. Zhu, T. Wu and K. Huang, A High Capacity Bilayer Cathode for Aqueous Zn-Ion Batteries, *ACS Nano*, 2019, **13**, 14447-14458.
47. P. He, G. Zhang, X. Liao, M. Yan, X. Xu, Q. An, J. Liu and L. Mai, Sodium Ion Stabilized Vanadium Oxide Nanowire Cathode for High-Performance Zinc-Ion Batteries, *Adv. Energy Mater.*, 2018, **8**, 1702463.
48. Y. Zhang, F. Wan, S. Huang, S. Wang, Z. Niu and J. Chen, A Chemically Self-Charging Aqueous Zinc-Ion Battery, *Nat. Commun.*, 2020, **11**, 2199.
49. L. Wang, K.-W. Huang, J. Chen and J. Zheng, Ultralong Cycle Stability of Aqueous Zinc-Ion Batteries with Zinc Vanadium Oxide Cathodes, *Sci. Adv.*, 2019, **5**, eaax4279.
50. N. Qiu, Z. Yang, R. Xue, Y. Wang, Y. Zhu and W. Liu, Toward a High-Performance Aqueous Zinc Ion Battery: Potassium Vanadate Nanobelts and Carbon Enhanced Zinc Foil, *Nano Lett.*, 2021, **21**, 2738-2744.
51. D. Kundu, B. D. Adams, V. Duffort, S. H. Vajargah and L. F. Nazar, A High-Capacity and Long-Life Aqueous Rechargeable Zinc Battery Using a Metal Oxide Intercalation Cathode, *Nat. Energ.*, 2016, **1**, 16119.
52. Y. Yang, Y. Tang, G. Fang, L. Shan, J. Guo, W. Zhang, C. Wang, L. Wang, J. Zhou and S. Liang, Li^+ Intercalated $V_2O_5{\cdot}nH_2O$ with Enlarged Layer Spacing and Fast Ion Diffusion as an Aqueous Zinc-Ion Battery Cathode, *Energy Environ. Sci.*, 2018, **11**, 3157-3162.
53. C. Xia, J. Guo, P. Li, X. Zhang and H. N. Alshareef, Highly Stable Aqueous Zinc-Ion Storage Using a Layered Calcium Vanadium Oxide Bronze Cathode, *Angew. Chem. Int. Ed.*, 2018, **57**, 3943-3948.
54. Y. Liu, Q. Li, K. Ma, G. Yang and C. Wang, Graphene Oxide Wrapped CuV_2O_6 Nanobelts as High-Capacity and Long-Life Cathode Materials of Aqueous Zinc-Ion Batteries, *ACS Nano*, 2019, **13**, 12081-12089.
55. Z. Cao, H. Chu, H. Zhang, Y. Ge, R. Clemente, P. Dong, L. Wang, J. Shen, M. Ye and P. M. Ajayan, An In Situ Electrochemical Oxidation Strategy for Formation of Nanogrid-Shaped $V_3O_7{\cdot}H_2O$ with Enhanced Zinc Storage Properties, *J. Mater. Chem. A.*, 2019, **7**, 25262-25267.
56. B. Tang, G. Fang, J. Zhou, L. Wang, Y. Lei, C. Wang, T. Lin, Y. Tang and S. Liang, Potassium

Vanadates with Stable Structure and Fast Ion Diffusion Channel as Cathode for Rechargeable Aqueous Zinc-Ion Batteries, *Nano Energy*, 2018, **51**, 579-587.
57. G. Su, S. Chen, H. Dong, Y. Cheng, Q. Liu, H. Wei, E. H. Ang, H. Geng and C. C. Li, Tuning the Electronic Structure of Layered Vanadium Pentoxide by Pre-Intercalation of Potassium Ions for Superior Room/Low-Temperature Aqueous Zinc-Ion Batteries, *Nanoscale*, 2021, **13**, 2399-2407.
58. T. Zhou, H. Xiao, L. Xie, Q. Han, X. Qiu, Y. Xiao, X. Yang, L. Zhu and X. Cao, Research on the Electrochemical Performance of Polyoxovanadate Material $K_4Na_2V_{10}O_{28}$ as a Novel AqueousZinc-Ion Batteries cathode, *Electrochim. Acta*, 2022, **424**, 140621.
59. H. Chen, W. Zhou, D. Zhu, Z. Liu, Z. Feng, J. Li and Y. Chen, Porous Cube-Like Mn_3O_4@C as an Advanced Cathode for Low-Cost Neutral Zinc-Ion Battery, *J. Alloys Compd.*, 2020, **813**, 151812.
60. D. Wang, L. Wang, G. Liang, H. Li, Z. Liu, Z. Tang, J. Liang and C. Zhi, A Superior δ-MnO_2 Cathode and a Self-Healing Zn-δ-MnO_2 Battery, *ACS Nano*, 2019, **13**, 10643-10652.
61. J. Wang, J.-G. Wang, H. Liu, Z. You, C. Wei and F. Kang, Electrochemical Activation of Commercial MnO Microsized Particles for High-Performance Aqueous Zinc-Ion Batteries, *J. Power Sources*, 2019, **438**, 226951.
62. X. Wu, Y. Xiang, Q. Peng, X. Wu, Y. Li, F. Tang, R. Song, Z. Liu, Z. He and X. Wu, Green-Low-Cost Rechargeable Aqueous Zinc-Ion Batteries Using Hollow Porous Spinel $ZnMn_2O_4$ as the Cathode Material, *J. Mater. Chem. A.*, 2017, **5**, 17990-17997.
63. S. Islam, M. H. Alfaruqi, V. Mathew, J. Song, S. Kim, S. Kim, J. Jo, J. P. Baboo, D. T. Pham, D. Y. Putro, Y.-K. Sun and J. Kim, Facile Synthesis and the Exploration of the Zinc Storage Mechanism of β-MnO_2 Nanorods with Exposed (101) Planes as a Novel Cathode Material for High Performance Eco-Friendly Zinc-Ion Batteries, *J. Mater. Chem. A.*, 2017, **5**, 23299-23309.
64. M. H. Alfaruqi, S. Islam, J. Gim, J. Song, S. Kim, D. T. Pham, J. Jo, Z. Xiu, V. Mathew and J. Kim, A High Surface Area Tunnel-Type α-MnO_2 Nanorod Cathode by a Simple Solvent-Free Synthesis for Rechargeable Aqueous Zinc-ion Batteries, *Chem. Phys. Lett.*, 2016, **650**, 64-68.
65. X. Wang, Z. Zhang, S. Xiong, F. Tian, Z. Feng, Y. Jia, J. Feng and B. Xi, A High-Rate and Ultrastable Aqueous Zinc-Ion Battery with a Novel $MgV_2O_6{\cdot}1.7H_2O$ Nanobelt Cathode, *Small*, 2021, **17**, 2100318.
66. T. Wu, K. Zhu, C. Qin and K. Huang, Unraveling the Role of Structural Water in Bilayer V_2O_5 During Zn^{2+}-Intercalation: Insights From DFT Calculations, *J. Mater. Chem. A.*, 2019, **7**, 5612-5620.
67. Z. Li, Y. Ren, L. Mo, C. Liu, K. Hsu, Y. Ding, X. Zhang, X. Li, L. Hu, D. Ji and G. Cao, Impacts of Oxygen Vacancies on Zinc Ion Intercalation in VO_2, *ACS Nano*, 2020, **14**, 5581-5589.
68. M. Du, C. Liu, F. Zhang, W. Dong, X. Zhang, Y. Sang, J. J. Wang, Y. G. Guo, H. Liu and S. Wang, Tunable Layered (Na,Mn)$V_8O_{20}{\cdot}nH_2O$ Cathode Material for High-Performance Aqueous Zinc Ion Batteries, *Adv. Sci.*, 2020, **7**, 2000083.